

Article

Bench-Scale Steam Reforming of Methane for Hydrogen Production

Hae-Gu Park ^{1,2}, Sang-Young Han ^{1,3}, Ki-Won Jun ^{1,3}, Yesol Woo ⁴, Myung-June Park ^{4,5,*}  and Seok Ki Kim ^{1,3,*}

¹ Carbon Resources Institute, Korea Research Institute of Chemical Technology, Daejeon 34114, Korea

² Department of Chemical and Biomolecular Engineering, Korea Advanced Institute of Science and Technology (KAIST), Daejeon 34141, Korea

³ Advanced Materials and Chemical Engineering, School of Science, Korea University of Science and Technology (UST), Yuseong, Daejeon 305-333, Korea

⁴ Department of Energy Systems Research, Ajou University, Suwon 16499, Korea

⁵ Department of Chemical Engineering, Ajou University, Suwon 16499, Korea

* Correspondence: mjpark@ajou.ac.kr (M.-J.P.); skkim726@kriect.re.kr (S.K.K.);
Tel.: +82-31-219-2895 (M.-J.P.); +82-42-860-7530 (S.K.K.)

Received: 5 July 2019; Accepted: 17 July 2019; Published: 20 July 2019



Abstract: The effects of reaction parameters, including reaction temperature and space velocity, on hydrogen production via steam reforming of methane (SRM) were investigated using lab- and bench-scale reactors to identify critical factors for the design of large-scale processes. Based on thermodynamic and kinetic data obtained using the lab-scale reactor, a series of SRM reactions were performed using a pelletized catalyst in the bench-scale reactor with a hydrogen production capacity of 10 L/min. Various temperature profiles were tested for the bench-scale reactor, which was surrounded by three successive cylindrical furnaces to simulate the actual SRM conditions. The temperature at the reactor bottom was crucial for determining the methane conversion and hydrogen production rates when a sufficiently high reaction temperature was maintained (>800 °C) to reach thermodynamic equilibrium at the gas-hourly space velocity of 2.0 L CH₄/(h·g_{cat}). However, if the temperature of one or more of the furnaces decreased below 700 °C, the reaction was not equilibrated at the given space velocity. The effectiveness factor (0.143) of the pelletized catalyst was calculated based on the deviation of methane conversion between the lab- and bench-scale reactions at various space velocities. Finally, an idling procedure was proposed so that catalytic activity was not affected by discontinuous operation.

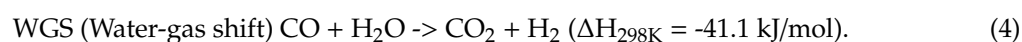
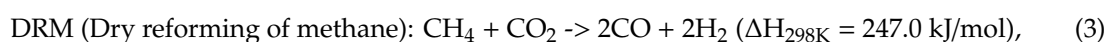
Keywords: methane steam reforming; hydrogen production; bench scale; effectiveness factor

1. Introduction

The demand for hydrogen has traditionally been high because hydrogen has been widely used as a chemical raw material in various refineries, as it is essential for the Fischer–Tropsch process and methanol synthesis [1,2]. Hydrogen is also expected to play an important role as a carbon-free energy carrier in the future [3,4]. Various methods for producing hydrogen with renewable energies have been proposed over the past few decades [5–13]. However, large-scale commercialization of hydrogen production using renewable energy to meet the massive demand for hydrogen remains challenging [14–16]. Until hydrogen production technology using renewable energy is sufficiently mature to facilitate the implementation of a sustainable hydrogen economy, a large amount of hydrogen is required to construct and operate the infrastructure for its storage, transportation, and utilization. Currently, steam reforming of fossil fuels or biomass is the most realistic option for producing large

amounts of hydrogen [17]. Among various resources, natural gas is abundant and inexpensive compared to other sources, and its reforming technologies are widely used on commercial scales [18].

Methane constitutes the majority of natural gas, but it is very stable and requires a significant energy input for utilization. The steam reforming of methane (SRM 1 and 2) is a strongly endothermic reaction, as shown in the reaction Equations (1) and (2), and it is usually operated at ≥ 800 °C. Here, the ratio of steam/methane is stoichiometrically 1, but steam is practically supplied at a ratio of ≥ 2.5 to prevent carbon deposition and improve the long-term stability of the catalyst. In addition, if excess water is supplied, a water–gas shift (WGS, Equation (4)) occurs despite its moderately exothermic nature, resulting in additional hydrogen production. As can be seen from Equations (1) and (2), the SRM is a volumetric expansion reaction, so the process is often operated at low pressure as it is thermodynamically preferred. However, to reduce the size of the reactor and facilitate the overall operation, the reactor is operated at a pressure of >0.5 MPa. Therefore, it is necessary to derive the optimal operating conditions according to the composition, amount of the desired product, and the process scale. Due to the small amount of CO_2 produced during the reaction, dry reforming of methane (DRM, Equation (3)) can also occur.



To date, most studies on SRM catalysts have focused on their activity and stability, which include studying the effect of the type and amount of active metal on catalyst performance and identifying the causes of deactivation, which include sintering of metallic species and coke deposition [19,20]. These studies have been performed in lab-scale reactors using powdered catalysts from a microscopic point of view. However, to increase the scale of the process, the catalyst must be pelletized to a certain size and shape considering the heat and mass transfer as well as the pressure drop in the reactor. Accordingly, the reactor and operating conditions must be properly engineered [21]. For catalysts used in commercial-scale reactors, their physicochemical properties must be first evaluated in a bench-scale process (or larger), and appropriate operating conditions must be derived. However, few studies have been performed on bench-scale reactions [22]. Herein, a commercial Ni-based catalyst was tested in lab- and bench-scale reactors, wherein powder- and pellet-type catalysts were used, respectively. We focused on determining the crucial factors of reactor design, especially for commercializing methane reforming reactions, by conducting a series of experiments under various conditions, including idling for intermittent operations.

2. Results and Discussion

2.1. Methane Steam Reforming Reaction in a Lab-Scale Reactor

Preliminary lab-scale reactions were performed using a powder-type catalyst obtained by grinding a commercial pellet-type catalyst and sieving it through a 16–20 size mesh. In the lab-scale reactor, the effects of reaction temperature, steam/methane ratio, and reaction pressure on SRM performance were studied. It should be noted that the temperature at the catalyst bed reported here was somewhat underestimated compared to the overall reactor system, so the experimental values could exceed the equilibrium values calculated based on the temperature of the catalyst bed. Figure 1a shows the effect of reaction temperature on methane conversion. For this reaction, the gas-hourly space velocity (GHSV) was fixed at $4.8 \text{ L CH}_4/(\text{h} \cdot \text{g}_{\text{cat}})$, the pressure was fixed at 1 MPa, and the steam/methane ratio was fixed at 3. As expected from the highly endothermic nature of the SRM (Equation (1)), methane conversion increased with reaction temperature. The experimental values of methane conversion were close to

equilibrium, indicating that the SRM reaction rate was not limited by the kinetics of the catalyst, but by the overall system thermodynamics.

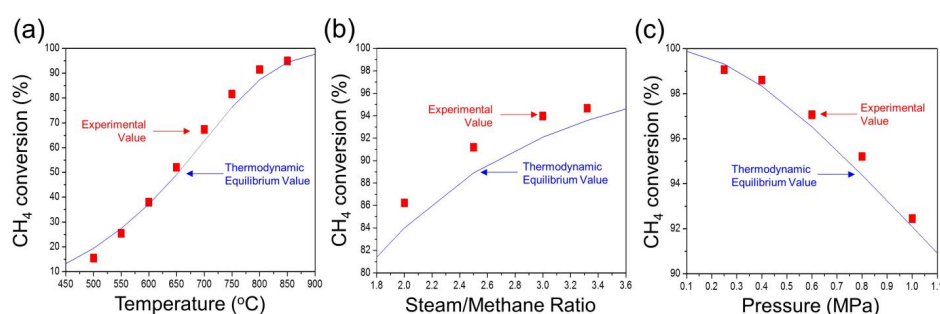


Figure 1. Effect of (a) reaction temperature, (b) steam/methane ratio, and (c) reaction pressure on methane conversion in the lab-scale reactor.

The effect of the steam/methane ratio on the methane conversion is shown in Figure 1b. For this reaction, the reaction temperature, pressure, and GHSV were fixed at 830 °C, 1 MPa, and 4.8 L CH₄/(h·g_{cat}), respectively. If the SRM is the only reaction taking place in the reactor, excessive steam does not necessarily affect methane conversion according to Equation (1). However, the increase in methane conversion as a function of steam/methane ratio suggests that an additional WGS (Equation (2)) also occurs, resulting in a shift in the SRM equilibrium so that methane consumption is accelerated at a higher steam/methane ratio [23].

Figure 1c shows the effect of the reaction pressure on methane conversion. For this reaction, the reaction temperature was fixed at 830 °C, the steam/methane ratio was fixed at 3, and GHSV was fixed at 4.8 L CH₄/(h·g_{cat}). The decreased methane conversion with increasing reaction pressure was in good agreement with the thermodynamic equilibrium conversion, indicating that the reaction rate was thermodynamically limited under the reaction conditions tested herein.

2.2. Methane Steam Reforming Reaction in a Bench-Scale Reactor

2.2.1. Effect of Reaction Temperature

The bench-scale SRM reaction was performed using a fixed-bed reactor, as shown in Figure 2. The reactor temperature was controlled by three heaters placed continuously. The inner diameter and length of the reactor were 32.52 mm and 110 cm, respectively. The temperature gradient along the vertical distance of the reactor was monitored using five thermocouples (TCs). The position of the TCs are shown in Figure 3.

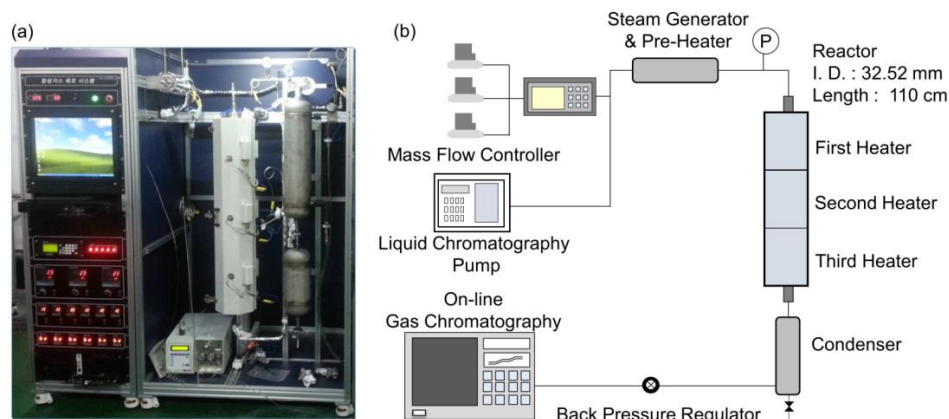


Figure 2. Bench-scale reaction system for the steam reforming of methane (hydrogen production rate of 10 L/min): (a) photograph of the unit and (b) schematic diagram of the unit.

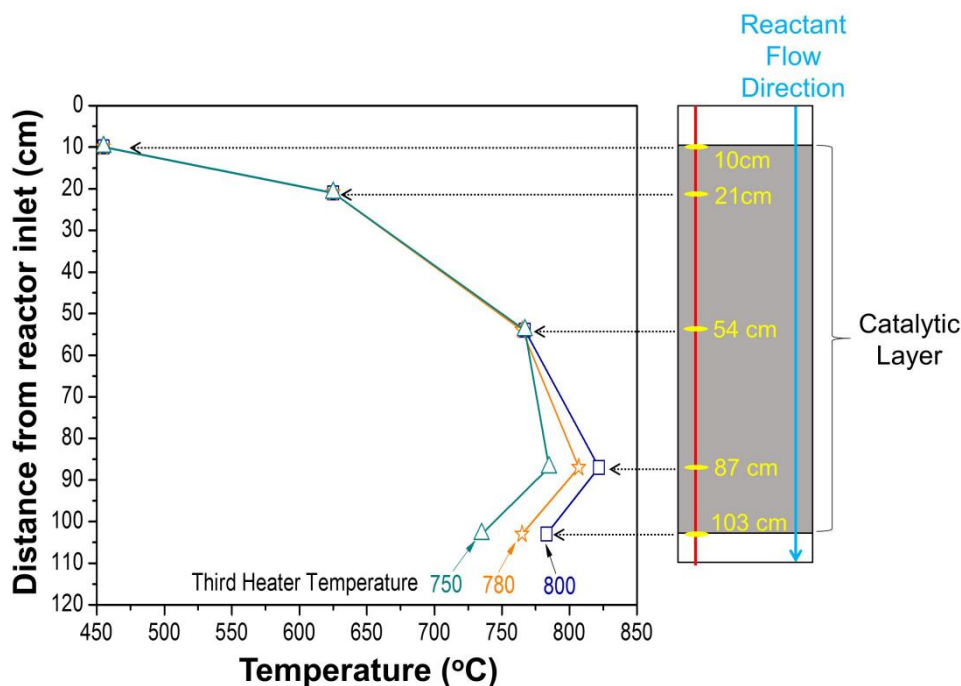


Figure 3. Temperature gradient along the catalyst bed depending on the third heater temperature (catalytic layer: 93 cm length, 96 g catalyst weight, 1386 g dilution agent weight, physical mixing). Schematic diagram of the reactor with the thermocouple (TC) positions (yellow bars) shown on the right-hand side.

The bench-scale reaction conditions were designed based on the lab-scale reaction results. The reaction was performed at a heater temperature of 800 °C, steam/methane ratio of 3, reaction pressure of 0.6 MPa, and GHSV of 2.0 L CH₄/(h·g_{cat}). To confirm whether the reaction set was close to the equilibrium state of the reforming reaction, the temperature of the bottom heater was changed to 800, 780, and 750 °C. The temperature profiles along the reactor distance and corresponding methane conversions are shown in Figure 3 and Table 1, respectively.

Table 1. Catalyst bed temperature gradient and CH₄ conversion at various third heater temperatures.

(a) Experimental Value						
3rd Heater	Temperature (°C)			CH ₄ Conversion (%)	Hydrogen Production Rate (L/min)	
	4th TC	5th TC	Mean Value (between the 4th and 5th TC)			
800	822	783	802.5	94.07	10.76	
780	807	764	785.5	92.43	10.68	
750	785	738	761.5	89.63	10.53	
(b) Thermodynamic Equilibrium Value						
Temperature (°C)			CH ₄ Conversion (%)			
750			87.10			
760			89.00			
770			90.67			
780			92.16			
790			93.46			
800			94.57			

Reaction conditions: steam/methane ratio = 3, feed composition of CH₄/H₂O/N₂ = 1/3/1, reaction pressure = 0.6 MPa, and gas-hourly space velocity (GHSV) = 2.0 L CH₄/(h·g_{cat}).

The results show that methane conversion decreased with decreasing bottom heater temperature. When the temperature of the bottom heater was maintained at 800, 780, and 750 °C, the methane conversions were 94.07%, 92.43%, and 89.63%, respectively. Accordingly, the hydrogen production rates were 10.76, 10.68, and 10.53 L/min, respectively. The methane conversion obtained for each condition is similar to the equilibrium conversion calculated based on the mean value of the temperature measured between the 4th and 5th TCs. For instance, when the mean temperature of 4th and 5th TCs was 802.5 °C, the bench reaction exhibited a methane conversion of 94.07% (Table 1a), which is close to the equilibrium conversion calculated at 800 °C (94.57%, in Table 1b). These results indicated that the SRM reaction rate was limited by the thermodynamic state that can be determined under the bench-reaction conditions. In addition, these results highlight the importance of the temperature at the bottom part of the reactor when the reaction is close to equilibrium.

The above reaction results were obtained under conditions that were sufficient to reach system equilibrium. However, in a commercial process, a more rapid temperature gradient would be expected depending on reactor design and climate conditions. Herein, two cases for the rapid temperature gradients that could be caused by heater malfunction were tested. In the first case, heat was assumed to be intensively supplied at the middle of the reactor. This is a typical scenario that can occur when the commercial side-fired reactor is operated in cold regions. The heater temperatures of those located at of the top, middle, and bottom were set to 600, 800, and 600 °C, respectively. In the second case, only the bottom heater was heated intensively, but the temperatures of the top and middle heaters were lowered to simulate another abnormal situation, where the extensive endothermic reaction takes place beyond the capacity of heaters. The temperatures of the top, middle, and bottom heaters were set to 500, 650, and 800 °C, respectively, for this scenario. These temperature profiles along with the catalyst bed distances are shown in Figure 4.

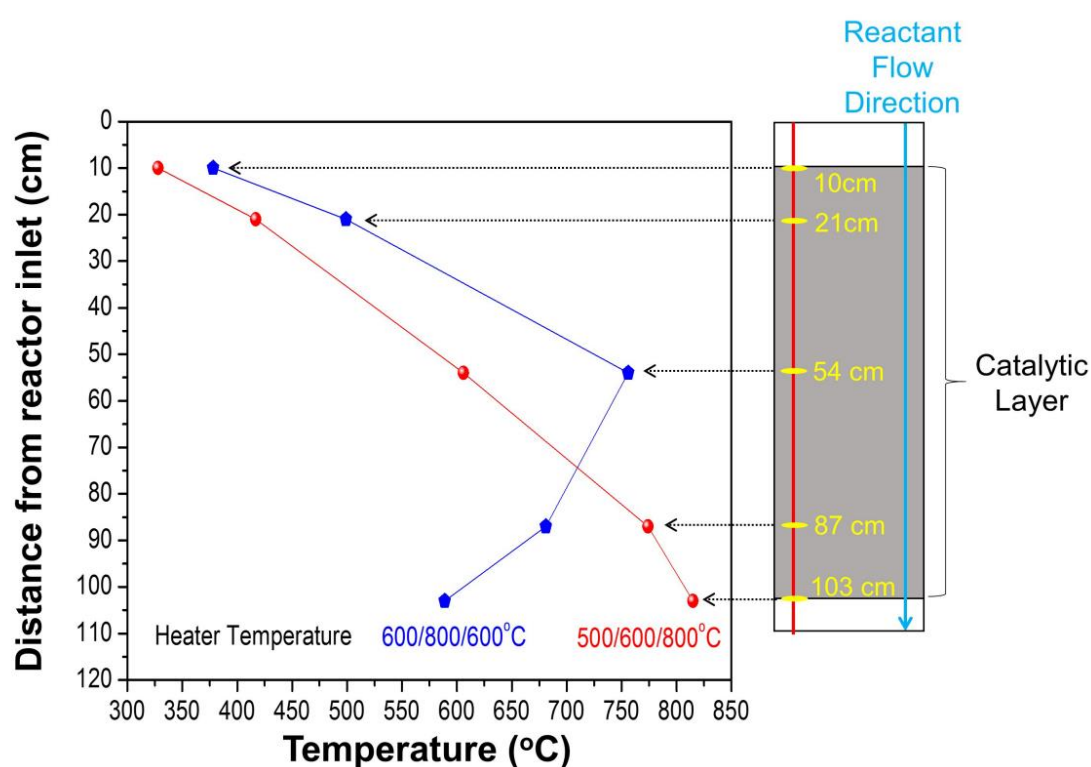


Figure 4. Temperature gradient along the catalyst bed under two abnormal conditions (catalytic layer: 93 cm length, 96 g catalyst weight, 1386 g dilution agent weight, and physical mixing).

The reaction results obtained under the two abnormal conditions are listed in Table 2. Methane conversion in the second scenario was 57.27%, which was ~7% lower than that obtained in the first scenario (64.13%). Given that the temperature of the bottom heater in the second scenario was higher

than that of the first, both SRM reactions were not under equilibrium conditions. This is in contrast to the cases listed in Table 2, where the SRMs were under equilibrium conditions as the top and middle heater temperatures were maintained at 800 °C.

Table 2. Catalyst bed temperature gradient and CH₄ conversion under abnormal conditions.

(a) Experimental Value			
Temperature (°C)			CH ₄ Conversion (%)
1st Heater	2nd Heater	3rd Heater	
500	650	800	57.27
600	800	600	64.13
(b) Thermodynamic Equilibrium Value			
Temperature (°C)			CH ₄ Conversion (%)
620			53.40
630			56.30
640			59.20
650			62.20
660			65.20
670			68.20

Reaction conditions: steam/methane ratio = 3, feed composition of CH₄/H₂O/N₂ = 1/3/1, reaction pressure = 0.6 MPa, and GHSV = 2.0 L CH₄/(h·g_{cat}).

The higher methane conversion in the first scenario was due to the wider region of the effective catalyst bed, which sufficiently maintained the reaction rate (>600 °C). However, in the second scenario where only the bottom heater temperature increased, the allowance for maintaining rapid catalysis was reduced. As a result, the space velocity was increased in the effective catalyst layer, consequently preventing the system from reaching equilibrium. To summarize, operation of the SRM reaction under equilibrium conditions can be achieved when supplying sufficient heat to the catalyst bed in as wide a manner as possible.

2.2.2. Effect of Space Velocity

As shown above, the reaction could not reach equilibrium if the reactor exhibited a sufficiently large temperature gradient because the space velocity was too fast for the catalyst to participate in the reaction. The effects of space velocity for different types of catalysts for the SRM reaction were investigated using lab- and bench-scale reactors, as shown in Figure 5. First, 0.15 g of a powdered catalyst 850 to 1250 μm in size was used in the lab-scale reactor, while 12 catalyst pellets (7.34 g) were used in the bench-scale reactor. For the latter reactor, the catalyst pellets were evenly distributed with 1440 g of alumina balls, and the length of the catalyst bed was 93.5 cm. The reaction was performed under various GHSV conditions at 800 °C for the three heaters, steam/methane ratio of 3, and reaction pressure of 0.6 MPa.

For both lab- and bench-scale reactions, methane conversion decreased with increasing space velocity, but the latter showed a larger decrease. That is, at a GHSV of 2.0 L CH₄/(h·g_{cat}), both experiments showed similar methane conversions (94.73% for the lab-scale and 91.52% for the bench-scale), but at a GHSV of 7.5 L CH₄/(h·g_{cat}), while the lab-scale reaction still showed a comparable methane conversion of 89.33%, that of the bench-scale reaction significantly decreased to 53.58%. This indicates that when the GHSV is ≥2.0 L CH₄/(h·g_{cat}), penetration of the reaction gas through the wall of the catalyst pellet does not occur to a sufficient extent, and the active component of the catalyst is not fully utilized, compared to the powdered catalyst. Accordingly, we suggest that the appropriate space velocity for hydrogen production in the bench-scale reaction should be ≤2.0 L CH₄/(h·g_{cat}). Based on the above results, the effectiveness factors of the pelletized catalysts were derived and the results reported in Section 2.2.3.

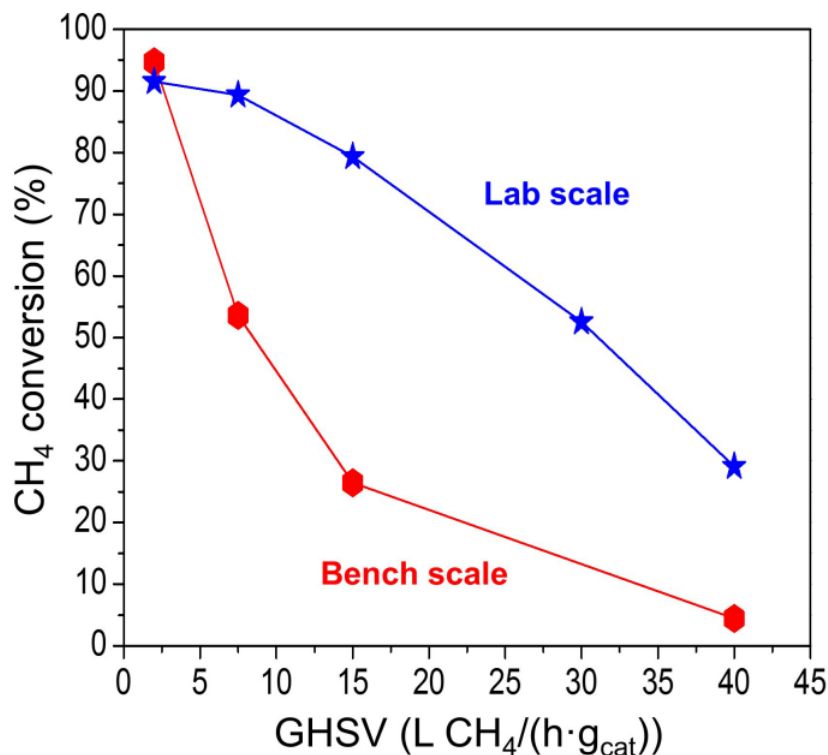


Figure 5. Methane conversion as a function of space velocity in the lab-scale and bench-scale reactors (reaction conditions: steam/methane ratio = 3, feed composition of CH₄/H₂O/N₂ = 1/3/1, reaction pressure = 0.6 MPa, and GHSV = 2.0–40.0 L CH₄/(h·g_{cat}).

2.2.3. Determination of the Effectiveness Factor

Determining an optimal catalyst loading in the reactor to maximize participation in the reaction is important when designing a large-scale reactor using pelletized catalysts. The effectiveness factor is defined as the ratio of the apparent reaction rate of the catalyst pellet to the intrinsic reaction rate, which provides information on the fraction of the catalyst pellet that participates in the reaction [24]. Based on experimental results for the lab- and bench-scale reactions, the effectiveness factor for the pelletized catalyst was determined. Instead of deriving all effectiveness factors for each individual reaction, the overall effectiveness factor ($\eta_{overall}$), as well as CO (SRM1) and CO₂ (SRM2) production from methane by steam reforming, dry reforming of methane (DRM), and the water–gas-shift reaction (WGS) were calculated as follows:

$$(r_{apparent})_i = \eta_{overall}(r_{intrinsic})_i \quad i = \text{SRM1, SRM2, DRM, WGS.} \quad (5)$$

To calculate the reaction rates for the commercial catalysts, $(r_{apparent})_i$, the reaction rates and kinetic parameters from our previous work were used without modification [25]:

$$r_{\text{SRM1}} = \frac{k_{\text{SRM1}}(f_{\text{CH}_4}f_{\text{H}_2\text{O}} - f_{\text{H}_2}^3f_{\text{CO}}/K_{\text{pSRM1}})/f_{\text{H}_2}^{2.5}}{[1 + K_{\text{CO}}f_{\text{CO}} + K_{\text{H}_2}f_{\text{H}_2} + K_{\text{CH}_4}f_{\text{CH}_4} + K_{\text{H}_2\text{O}}(f_{\text{H}_2\text{O}}/f_{\text{H}_2})]^2}; \quad (6)$$

$$r_{\text{SRM1}} = \frac{k_{\text{SRM1}}(f_{\text{CH}_4}f_{\text{H}_2\text{O}} - f_{\text{H}_2}^3f_{\text{CO}}/K_{\text{pSRM1}})/f_{\text{H}_2}^{2.5}}{[1 + K_{\text{CO}}f_{\text{CO}} + K_{\text{H}_2}f_{\text{H}_2} + K_{\text{CH}_4}f_{\text{CH}_4} + K_{\text{H}_2\text{O}}(f_{\text{H}_2\text{O}}/f_{\text{H}_2})]^2}; \quad (7)$$

$$r_{\text{DRM}} = \frac{k_{\text{DRM}}(f_{\text{CH}_4}f_{\text{CO}_2} - f_{\text{H}_2}^2f_{\text{CO}}^2/K_{\text{pDRM}})}{(1 + K_{\text{CH}_4}f_{\text{CH}_4} + K_{\text{CO}}f_{\text{CO}})(1 + K_{\text{CO}_2}f_{\text{CO}_2})}; \quad (8)$$

$$r_{\text{WGS}} = \frac{k_{\text{WGS}}(f_{\text{CO}}f_{\text{H}_2\text{O}} - f_{\text{H}_2}f_{\text{CO}_2}/K_{\text{pWGS}})/f_{\text{H}_2}}{\left[1 + K_{\text{CO}}f_{\text{CO}} + K_{\text{H}_2}f_{\text{H}_2} + K_{\text{CH}_4}f_{\text{CH}_4} + K_{\text{H}_2\text{O}}(f_{\text{H}_2\text{O}}/f_{\text{H}_2})\right]^2}; \quad (9)$$

where k_i and K_i denote the reaction rate constant and adsorption equilibrium constants, respectively, for species i . Fugacity (f) was calculated using the generalized correlations for the fugacity coefficient, as described in the literature [26]. The symbol K_p represents the reaction equilibrium constant, which was obtained from the process simulator UniSim Design Suite R400 (Honeywell Inc., Charlotte, NC, USA)

Because the inert fraction of the catalyst bed was extremely high (7.34 g of catalyst pellet and 1440 g of inert materials) in the bench-scale reactor, a catalyst pellet was considered to be a single reactor module in the process simulator, as shown in Figure 6a, 12 of which were connected consecutively over the entire packing of the reactor. Figure 6b shows a comparison of the methane conversion between the experimental data and simulated results, where the simulated values coincide with the observed data satisfactorily (mean of absolute relative residuals (MARRs) and relative standard deviation were 26.7% and 2.23%, respectively, for GHSV values of 7.5 and 15.0 L CH₄/(h·g_{cat}), when the value at 40.0 mL CH₄/(h·g_{cat}) was excluded as an outlier).

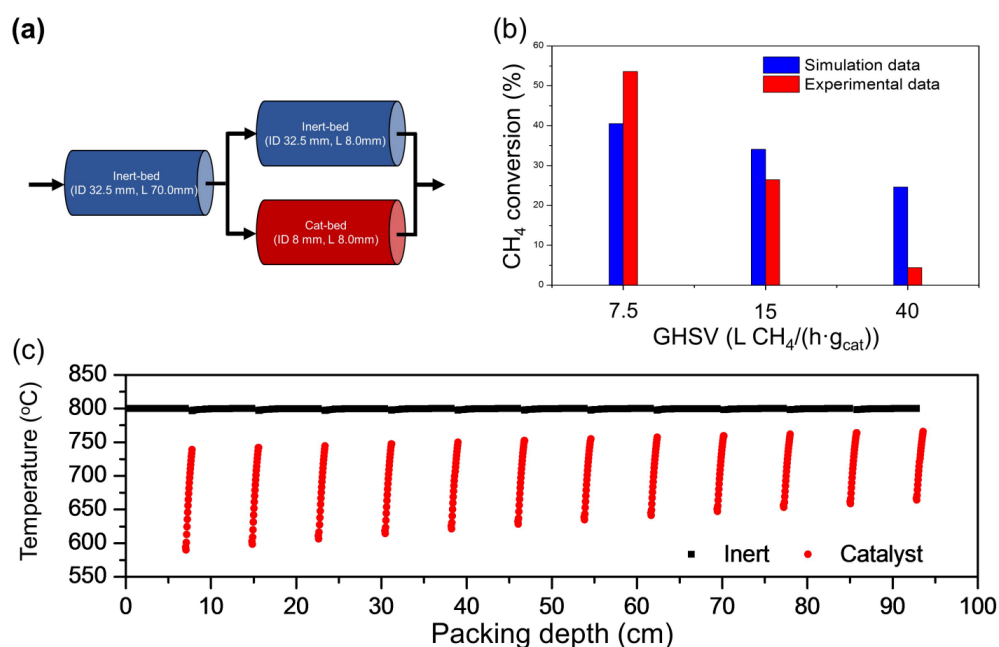


Figure 6. (a) Schematic of the bench-scale reactor (hydraulic diameter of the catalyst pellet was used in the Cat-bed module), (b) comparison of the CH₄ conversion for various space velocities [mL CH₄/(h·g_{cat})], and (c) temperature profile in the reactor at 7.5 L CH₄/(h·g_{cat}). Wall temperature = 800 °C, pressure = 0.6 MPa, overall heat transfer coefficient = 100 W/(m²·K), and feed composition of CH₄/H₂O/N₂ = 1/3/1.

For the lab-scale reactor, a single plug flow reactor (PFR) was used in the simulator, and a reaction rate of $(r_{\text{intrinsic}})_i = (r_{\text{apparent}})_i / \eta_{\text{overall}}$ was used. Figure 7a shows the MARR values for CH₄ conversion as a function of η_{overall} , where the optimal value of η_{overall} was 0.143 for the minimum MARR (18.8%). Figure 7b shows that the simulated values of CH₄ conversion agreed well with the experimental data for various space velocities. The temperature profile was also estimated, as shown in Figure 7c. The reaction temperature decreased to ~600 °C at the initial part of the catalyst bed and increased gradually due to heat transfer from the wall, resulting in the exit temperature being close to that of the wall.

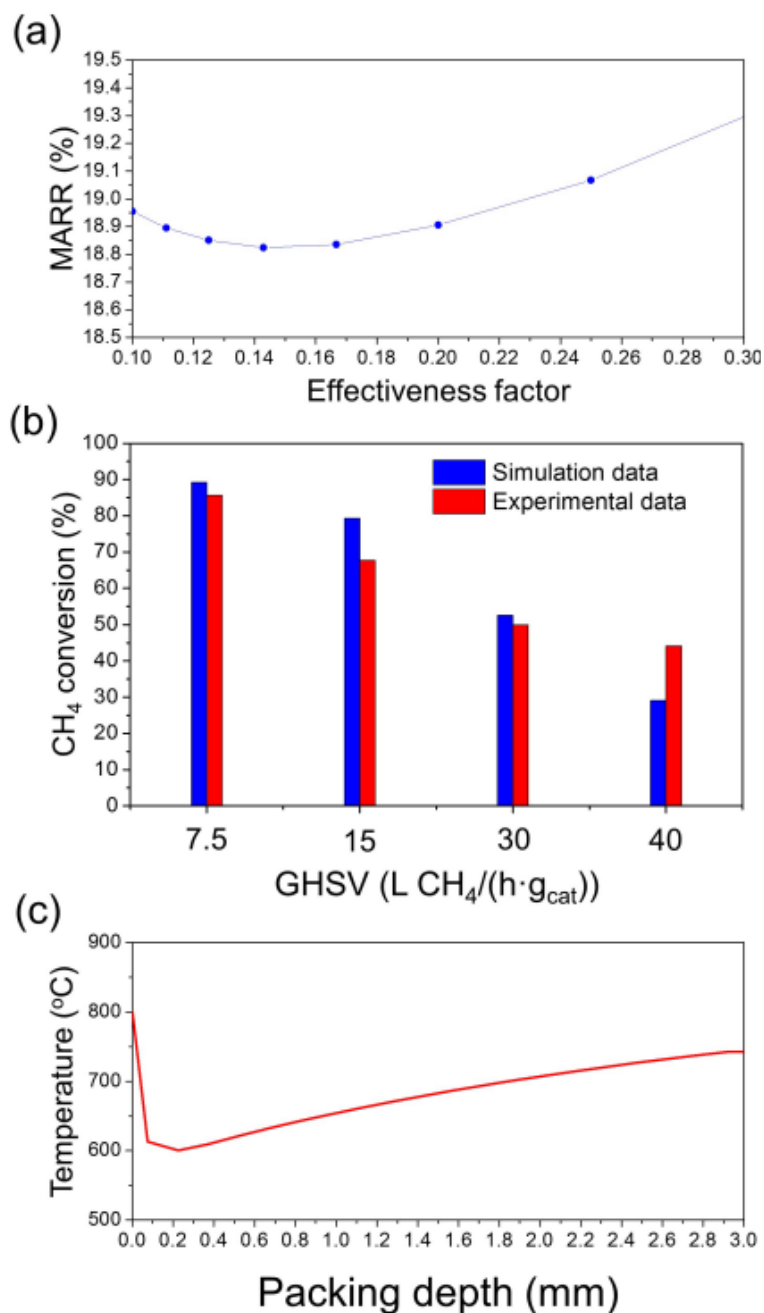


Figure 7. (a) Mean of absolute relative residuals (MARRs) values with respect to the overall effectiveness factor, (b) comparison of CH₄ conversion for various space velocities [mL CH₄/(h·g_{cat})], (c) temperature profile in the reactor at 7500 mL CH₄/(h·g_{cat}). Wall temperature = 800 °C, pressure = 0.6 MPa, overall heat transfer coefficient = 100 W/m²·K, and feed composition of CH₄/H₂O/N₂ = 1/3/1.

2.3. Idling Conditions

In addition to the extreme temperature gradient of the heaters, a stable idling condition was also simulated under the assumption of discontinuous power supply. The activity of the catalyst can be maintained by maintaining stable idling conditions. By applying an effective idling operation to the process, the reaction may not be completely terminated, which would shorten the preparation time for restarting the operation.

Figure 8 shows temperatures recorded along the SRM reaction followed by idling operation and the restart process. In a typical starting procedure, the reactor containing a reduced catalyst was heated to the reaction temperature (800 °C, region (1) in Figure 8b) prior to feeding the reactants.

After stabilizing the reactor temperature, the SRM reaction was initiated by feeding the reactants (region (2)). After completion of the reaction, the three heaters were maintained at 500 °C, and nitrogen flowed inside the reactor at a rate of 1 L/min (region (3)). When the reforming reaction proceeded again, the reactor temperature was heated (region ((4) followed by feeding of the reactants (region (5)). As shown in Table 3, no significant changes in catalytic performance were observed before or after the idling operation.

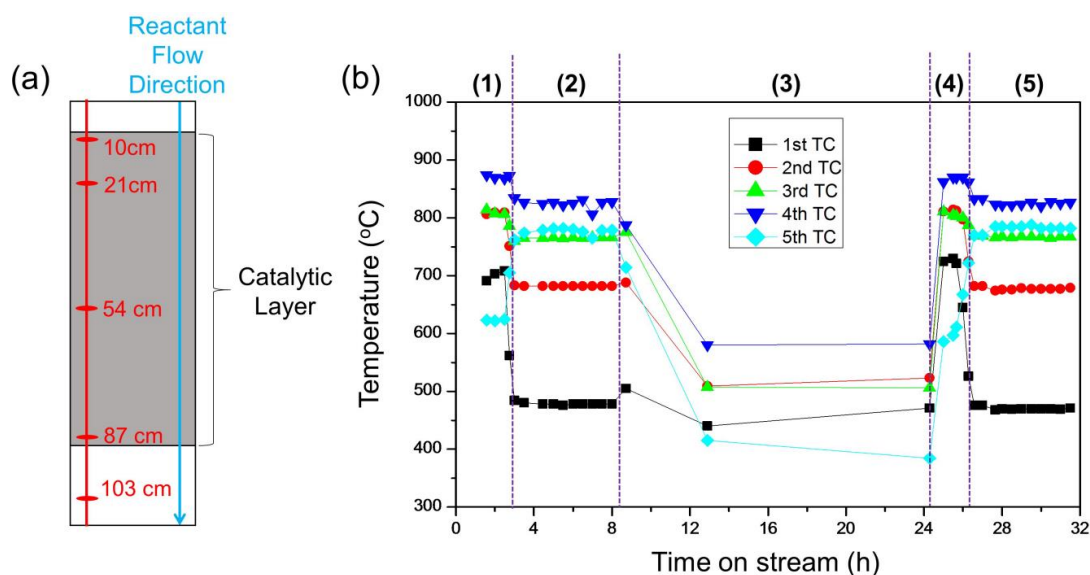


Figure 8. (a) Schematic of a catalytic layer for idling operation, (b) temperature recorded before (1, 2), during (3), and after idling (4, 5).

Table 3. Comparison of temperature, methane conversion, and hydrogen production before and after idling.

	Temperature (°C)					CH ₄ Conversion (%)	Rate of Hydrogen Production (L/min)
	1st TC	2nd TC	3rd TC	4th TC	5th TC		
Before idling	478	682	766	826	781	92.95	6.67
After idling	469	677	767	825	782	92.81	6.65

Reaction conditions: steam/methane ratio = 3, feed composition of CH₄/H₂O/N₂ = 1/3/1, reaction pressure = 0.6 MPa, GHSV = 2.0 L CH₄/(h·g_{cat}), catalytic layer = 82 cm length, catalyst weight = 80 g, dilution agent weight = 1220 g, and physical mixing.

3. Materials and Methods

3.1. Catalyst Characterization

As a preliminary study for applying a pelletized catalyst to a commercial process, reactions were performed using a commercial Ni-based catalyst suitable for mass production of hydrogen. The textural properties and composition of the catalyst are listed in Table 4.

Table 4. Textural properties of the catalyst used herein.

Parameters	Data
Shape	1-hole cylinder
Size	O.D. 8.17 mm, I.D. 2.85 mm, Height 7.21 mm
Composition	Ni 20 wt.%, CaO-Al ₂ O ₃ 80 wt.%
Density	1.80 g/cm ³
Packing Density (in bench reactor)	0.718 g/cm ³
Surface Area	21.26 m ² /g
Micropore Area	13.07 m ² /g
Pore Volume	0.033 cm ³ /g
Pore Size	111 Å

For structural characterization, the commercial catalyst was ground and meshed to a size of ≤ 250 μm . The Brunauer–Emmett–Teller (BET) specific surface area, micropore area, pore volume, and pore size distribution of the powdered catalyst were estimated from the N₂ adsorption and desorption isotherm obtained at -195.7 °C using a constant-volume adsorption apparatus (Micromeritics, ASAP-2020, Norcross, GA, USA). The pore volumes were determined at a relative pressure (P/P_0) of 0.99. The catalyst was degassed at 300 °C for 4 h before the measurements. The pore size distributions of the samples were calculated using the Barrett–Joyner–Halenda (BJH) model.

3.2. Steam Reforming Reaction

3.2.1. Methane Steam Reforming Reaction in the Lab-Scale Reactor

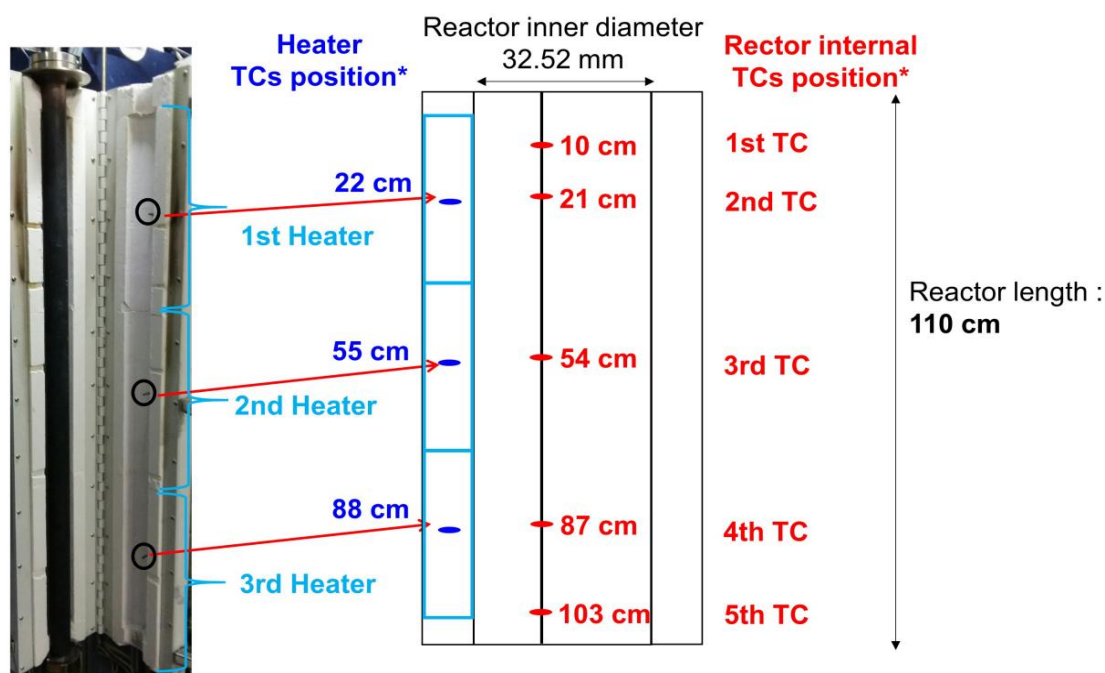
The catalytic activity of the powdered catalyst for the methane steam reforming reaction was tested in a fixed-bed tubular Inconel reactor (ID = 10 mm). Prior to feeding the reactants, the catalyst was activated by flowing H₂ at a rate of 50 mL/min at 800 °C for 120 min. A TC was placed at the center of the catalyst bed to monitor the reaction temperature, and the feed flow was controlled using a mass flow controller (Brooks, 5850E, Hatfield, PA, USA). The gas products were analyzed using an online gas chromatograph (GC) (Young Lin Acme 6000, Gyeonggi-do, Korea) with a 40/60 carboxen-1000 column (2.0 ft \times 1/8 in. \times 2.1 mm) and a thermal conductivity detector (TCD). Nitrogen was used as an internal standard gas to verify the composition of the analytical gas (methane) as a volume or half volume.

The activity data shown in Figure 1 were collected by varying the reaction temperature (500 to 850 °C), steam/methane ratio (2 to 3.3), and reaction pressure (0.2 to 1 MPa). The methane conversions shown in Figure 5 (lab-scale) were evaluated under the following reaction conditions: heater temperature = 800 °C; pressure = 0.6 MPa; steam/methane ratio = 3; feed composition of CH₄/H₂O/N₂ = 1/3/1; and gas hourly space velocity (GHSV) = 2.0–40.0 L CH₄/(h·g_{cat}).

The equilibrium conversion was calculated using “HSC chemistry” software (Outotec, Espoo, Finland).

3.2.2. Methane Steam Reforming Reaction in the Bench-Scale Reactor

The bench-scale reactor consisted of three heaters, a stainless-steel reactor with an inner diameter of 32.52 mm and length of 110 cm, and five TCs. Figure 9 shows the bench reactor in detail. The TCs of the three heaters were located 22, 55, and 88 cm from the reactor inlet. Five TCs were located inside the reactor to monitor the temperature of the catalyst bed, at positions of 10, 21, 54, 87, and 103 cm. To prevent localization of heat and mass, the reactor was filled with a mixture of a pellet-type catalyst and spherical diluent (alpha-alumina). Prior to the SRM reaction, the catalyst mixture was activated by flowing H₂ at a rate of 1 L/min at 800 °C for 120 min. The experiment was conducted under the conditions mentioned above, and the analysis method was the same as that of the lab-scale reaction.



*Position: Distance from reactor inlet

Figure 9. Detailed position of the heaters and TCs in the bench-scale reactor.

4. Conclusions

A series of lab- and bench-scale SRM experiments were performed to identify and solve the problems that could occur during scale-up. In the lab-scale reaction, the effects of temperature, pressure, and steam/methane ratio on methane conversion were investigated in comparison to the corresponding equilibrium conversion. Based on the lab-scale experiments, a bench-scale reaction was designed. The methane conversion in the bench-scale reactor was >90%, and the hydrogen production was >10 L/min if the three consecutive heaters sufficiently supplied the heat required to reach the equilibrium (>800 °C). Under these conditions, the heater temperature positioned at the bottom of the reactor (outlet side) largely governed the methane conversion. Under abnormal reactor temperature conditions, where the catalyst bed was not heated sufficiently (<650 °C), the reaction was not equilibrated simply by maintaining the temperature of the bottom heater at 800 °C. This is similar to the case where the space velocity is relatively high (>10.0 L CH₄/(h·g_{cat})). Using kinetic data obtained from the lab- and bench-scale reactions, the effective factor (0.143) for the pelletized catalysts was calculated. Finally, we proposed effective idling operating conditions that prevented catalyst deactivation during process downtime and reduced the time and costs involved in restarting the process.

Author Contributions: H.-G.P., K.-W.J., and S.K.K. conceived and designed the experiments; H.-G.P. and S.-Y.H. performed the experiments; Y.W. and M.-J.P. analyzed and simulated the data; S.K.K. administrated the project; H.-G.P. wrote original draft; M.-J.P. and S.K.K. reviewed and modified the manuscript.

Funding: This work was supported by the Korea Gas Corporation R&D program (Project No. IPT17-12) and Korea Research Institute of Chemical Technology (Project No. SI1911-60).

Acknowledgments: We thank Jin-Mo Park and Hyung-Sik Kim of Korea Gas Corporation for helpful discussion on this work.

Conflicts of Interest: The authors declare no conflict of interest.

References

1. Iglesia, E. Design, synthesis, and use of cobalt-based Fischer-Tropsch synthesis catalysts. *Appl. Catal. A Gen.* **1997**, *161*, 59–78. [[CrossRef](#)]
2. Zhang, C.; Jun, K.-W.; Kwak, G.; Lee, Y.-J.; Park, H.-G. Efficient utilization of carbon dioxide in a gas-to-methanol process composed of CO₂/steam mixed reforming and methanol synthesis. *J. CO₂ Util.* **2016**, *16*, 1–7. [[CrossRef](#)]
3. Prater, K.B. Polymer electrolyte fuel cells: A review of recent developments. *J. Power Sources* **1994**, *51*, 129–144. [[CrossRef](#)]
4. Minh, N.Q. Ceramic Fuel Cells. *J. Am. Ceram. Soc.* **1993**, *76*, 563–588. [[CrossRef](#)]
5. Nagaoka, K.; Eboshi, T.; Takeishi, Y.; Tasaki, R.; Honda, K.; Imamura, K.; Sato, K. Carbon-free H₂ production from ammonia triggered at room temperature with an acidic RuO₂/gamma-Al₂O₃ catalyst. *Sci. Adv.* **2017**, *3*, e1602747. [[CrossRef](#)] [[PubMed](#)]
6. Hill, A.K.; Torrente-Murciano, L. Low temperature H₂ production from ammonia using ruthenium-based catalysts: Synergetic effect of promoter and support. *Appl. Catal. B Environ.* **2015**, *172*, 129–135. [[CrossRef](#)]
7. Cheng, C.; Shi, J.; Hu, Y.; Guo, L. WO₃/g-C₃N₄ composites: One-Pot preparation and enhanced photocatalytic H₂ production under visible-light irradiation. *Nanotechnology* **2017**, *28*, 164002. [[CrossRef](#)]
8. Ouyang, S.; Tong, H.; Umezawa, N.; Cao, J.; Li, P.; Bi, Y.; Zhang, Y.; Ye, J. Surface-alkalinization-induced enhancement of photocatalytic H₂ evolution over SrTiO₃-based photocatalysts. *J. Am. Chem. Soc.* **2012**, *134*, 1974–1977. [[CrossRef](#)]
9. Qin, J.; Huo, J.; Zhang, P.; Zeng, J.; Wang, T.; Zeng, H. Improving the photocatalytic hydrogen production of Ag/g-C₃N₄ nanocomposites by dye-sensitization under visible light irradiation. *Nanoscale* **2016**, *8*, 2249–2259. [[CrossRef](#)]
10. Lindgren, M.; Panas, I. Confinement dependence of electro-catalysts for hydrogen evolution from water splitting. *Beilstein. J. Nanotechnol.* **2014**, *5*, 195–201. [[CrossRef](#)]
11. Yildiz, B.; Kazimi, M.S. Efficiency of hydrogen production systems using alternative nuclear energy technologies. *Int. J. Hydrogen Energy* **2006**, *31*, 77–92. [[CrossRef](#)]
12. Nagasawa, K.; Davidson, F.T.; Lloyd, A.C.; Webber, M.E. Impacts of renewable hydrogen production from wind energy in electricity markets on potential hydrogen demand for light-duty vehicles. *Appl. Energy* **2019**, *235*, 1001–1016. [[CrossRef](#)]
13. Sarma, S.J.; Brar, S.K.; Sydney, E.B.; Le Bihan, Y.; Buelna, G.; Soccol, C.R. Microbial hydrogen production by bioconversion of crude glycerol: A review. *Int. J. Hydrogen Energy* **2012**, *37*, 6473–6490. [[CrossRef](#)]
14. Turner, J.A. Sustainable hydrogen production. *Science* **2004**, *305*, 972–974. [[CrossRef](#)] [[PubMed](#)]
15. Szima, S.; Nazir, S.M.; Cloete, S.; Amini, S.; Fogarasi, S.; Cormos, A.-M.; Cormos, C.-C. Gas switching reforming for flexible power and hydrogen production to balance variable renewables. *Renew. Sustain. Energy Rev.* **2019**, *110*, 207–219. [[CrossRef](#)]
16. Rashid, M.M.; Al Mesfer, M.K.; Naseem, H.; Danish, M. Hydrogen production by water electrolysis: A review of alkaline water electrolysis, PEM water electrolysis and high temperature water electrolysis. *Int. J. Eng. Adv. Technol.* **2015**, *4*, 80–93.
17. Barelli, L.; Bidini, G.; Gallorini, F.; Servili, S. Hydrogen production through sorption-enhanced steam methane reforming and membrane technology: A review. *Energy* **2008**, *33*, 554–570. [[CrossRef](#)]
18. Zamaniyan, A.; Ebrahimi, H.; Mohammadzadeh, J.S.S. A unified model for top fired methane steam reformers using three-dimensional zonal analysis. *Chem. Eng. Process. Process. Intensif.* **2008**, *47*, 946–956. [[CrossRef](#)]
19. Wu, H.; Parola, V.L.; Pantaleo, G.; Puleo, F.; Venezia, A.M.; Liotta, L.F. Ni-Based Catalysts for low temperature methane steam reforming: Recent results on Ni-Au and comparison with other bi-metallic systems. *Catalysts* **2013**, *3*, 563–583. [[CrossRef](#)]
20. Liu, C.-J.; Ye, J.; Jiang, J.; Pan, Y. Progresses in the preparation of coke resistant Ni-based catalyst for steam and CO₂ reforming of methane. *Chem. Cat Chem.* **2011**, *3*, 529–541. [[CrossRef](#)]
21. Mohammadzadeh, J.S.S.; Zamaniyan, A. Catalyst shape as a design parameter—Optimum shape for methane-steam reforming catalyst. *Chem. Eng. Res. Des.* **2002**, *80*, 383–391. [[CrossRef](#)]
22. Saric, M.; Delft, Y.C.; Sumbharaju, R.; Meyer, D.F.; Groot, A. Steam reforming of methane in a bench-scale membrane reactor at realistic working conditions. *Catal. Today* **2012**, *193*, 74–80. [[CrossRef](#)]

23. Wang, Y.; Chin, Y.H.; Rozmiarek, R.T.; Johnson, B.R.; Gao, Y.; Watson, J.; Tonkovich, A.Y.L.; Vander Wiel, D.P. Highly active and stable Rh/MgO–Al₂O₃ catalysts for methane steam reforming. *Catal. Today* **2004**, *98*, 575–581. [[CrossRef](#)]
24. Baek, S.M.; Kang, J.H.; Lee, K.-J.; Nam, J.H. A numerical study of the effectiveness factors of nickel catalyst pellets used in steam methane reforming for residential fuel cell applications. *Int. J. Hydrogen Energy* **2014**, *39*, 9180–9192. [[CrossRef](#)]
25. Park, N.; Park, M.-J.; Baek, S.-C.; Ha, K.-S.; Lee, Y.-J.; Kwak, G.; Park, H.-G.; Jun, K.-W. Modeling and optimization of the mixed reforming of methane: Maximizing CO₂ utilization for non-equilibrated reaction. *Fuel* **2014**, *115*, 357–365. [[CrossRef](#)]
26. Smith, J.M.; Van Ness, H.C.; Abbott, M.M. *Introduction to Chemical Engineering Thermodynamics*, 7th ed.; McGraw-Hill: New York, NY, USA, 2005.



© 2019 by the authors. Licensee MDPI, Basel, Switzerland. This article is an open access article distributed under the terms and conditions of the Creative Commons Attribution (CC BY) license (<http://creativecommons.org/licenses/by/4.0/>).